

Cooperative molecular motors moving back and forth

David Gillo^{1†}, Barak Gur^{2†},

Anne Bernheim-Groswasser¹ and Oded Farago³

¹Department of Chemical Engineering, ²Department of Physics,

³Department of Biomedical Engineering

Ben Gurion University, Be'er Sheva 84105, Israel

August 14, 2018

Abstract

We use a two-state ratchet model to study the cooperative bidirectional motion of molecular motors on cytoskeletal tracks with randomly alternating polarities. Our model is based on a previously proposed model [Badoual et al., *Proc. Natl. Acad. Sci. USA* **99**, 6696 (2002)] for collective motor dynamics and, in addition, takes into account the cooperativity effect arising from the elastic tension that develops in the cytoskeletal track due to the joint action of the walking motors. We show, both computationally and analytically, that this additional cooperativity effect leads to a dramatic reduction in the characteristic reversal time of the bidirectional motion, especially in systems with a large number of motors. We also find that bidirectional motion takes place only on (almost) a-polar tracks, while on even slightly polar tracks the motion is unidirectional. We argue that the origin of these observations is the sensitive dependence of the cooperative dynamics on the difference between the number of motors typically working in and against the instantaneous direction of motion.

[†] Authors with equal contributions

1 Introduction

Many cellular processes such as cell motility and mitosis require the cooperative work of many motors in order to preserve continuous motion and force generation [1]. Muscle contraction, for example, involves the simultaneous action of hundreds of myosin II motors pulling on attached actin filaments and causing them to slide against each other [2]. Groups of myosin II motors are also responsible for the contraction of the contractile ring during cytokinesis [3]. In certain biological systems, cooperative behavior of molecular motors produces oscillatory motion. In some insects, for instance, cooperative behavior of molecular motors leads to oscillations of the flight muscles [4]. Another example is the oscillatory motion of axonemal cilia and flagella, which is believed to be generated by a large number of interacting dynein motors [5,6]. Finally, cooperative action of motors is required for the extraction of membrane tubes from vesicles [7,8]

One of the more interesting outcomes of cooperative action of molecular motors is their ability to induce bidirectional motion. “Back and forth” dynamic has been observed in various motility assays including: (i) myosin II motors walking on actin tracks with randomly alternating polarities [9], (ii) NK11 (kinesin related Ncd mutants which individually exhibit random motion with no preferred directionality) moving on microtubules (MTs) [10], (iii) mixed population of plus-end (kinesin-5 KLP61F) and minus-end (Ncd) driven motors acting on MTs [11], and (iv) myosin II motors walking on actin filaments in the presence of external stalling forces [12]. Reversible transport of organelles through the combined action of kinesin II, dynein, and myosin V has been also observed in *Xenopus* melanophores [13]. In the latter example, the kinesin and dynein move the organelle in opposite directions along MTs, while the myosin motors (which take the organelle on occasional “detours” along the actin filaments) function as “molecular ratchets”, controlling the directionality of the movement along the MT transport system. From a theoretical point of view, cooperative dynamics of molecular motors and, in particular, bidirectional movement, have been investigated using several distinct models. These models include: (i) lattice and continuum asymmetric exclusion models [14–20], (ii) ratchet models of *interacting* particles moving in the presence of a periodic potential [16,21–24], and (iii) the tug-of-war model which has been recently proposed for describing the transport of cargo by the action of a few motors [25–28]. The common theme in these experimental and theoretical studies is the association of bidirectionality with the competition between two populations of motors that work against each other to drive the system in opposite directions. The occasional reversals of the transport direction reflect the “victory” of one group over the other during the respective time intervals. The balance of power is shifting between the two motor parties as a result of stochastic events of binding and unbinding of motors to the cytoskeletal track. Without going into the details of the various existing models of cooperative bidirectional motion, we note that most of them assume that the motors interact mechanically but act independently, i.e., their binding to and unbinding from the track are uncorrelated. By further assuming that the attachment and detachment events of individual motors are Markovian, the distribution of “reversal times” (i.e., the durations of unidirectional intervals of motion) can be shown to take an exponential form

$$p(\delta t) = \exp(-\delta t/\tau_{\text{rev}}), \quad (1)$$

where τ_{rev} is the characteristic reversal time of the bidirectional motion.

The magnitude of τ_{rev} can be taken as a measure for the degree of cooperativity between

the motors. The more cooperative the motors are, the more persistent is the movement and the longer are the periods of unidirectional transport. The run lengths (in each direction) of highly cooperative motors may be of a few microns even for non-processive motors like myosin II [9]. As noted above, the mechanical coupling between the motors is sufficient for the generation of highly cooperative bidirectional motion, even if the motors attach to/detach from the track in an uncorrelated fashion. This has been demonstrated theoretically by Badoual *et al.* some years ago [23]. A slightly modified version of this model is illustrated schematically in Fig. 1. The model considers the one-dimensional motion of a group of N point particles (representing the motors) connected (mechanically coupled) to a rigid rod with equal spacing q . The cytoskeletal track is represented by a periodic saw-tooth potential, $U(x)$, with period l and height H . The model requires that q is larger than and incommensurate with l . The motors are identical and walk on a track which is globally a-polar and, thus, does not permit net transport to the right or left over large time scales. The temporal direction of motion is determined by the net force generated by all the motors. The local polarity of the track is represented by an additional force of size f_{ran} (denoted by a horizontal arrow in each periodic unit in Fig. 1) which, within each unit of the periodic potential, points to the right or to the left. The globally a-polar nature of the track is ensured by requiring that the sum of these random forces vanishes.

The instantaneous force between the track and the motors is given by the sum of all the forces acting on the individual motors:

$$F_{\text{tot}} = \sum_{i=1}^N f_i^{\text{motor}} = \sum_{i=1}^N \left[-\frac{\partial U(x_1 + (i-1)q)}{\partial x} + f_{\text{ran}}(x_1 + (i-1)q) \right] \cdot C_i(t), \quad (2)$$

where $x_i = x_1 + (i-1)q$ is the coordinate of the i -th motor. The two terms in the square brackets represent the forces due to the symmetric saw-tooth potential and the additional random local forces acting in each periodic unit. The function $C_i(t)$ takes two possible values, 0 or 1, depending on whether the motor i is detached from or attached to the track, respectively, at time t . The motors change their binding states (0 - detached; 1 - attached) independently of each other, according to the following rules: We define an interval of size $2a < l$ centered around the potential minima (the gray shaded area in Fig. 1). If located in one of these regions, an attached motor may become detached ($1 \rightarrow 0$) with a probability per unit time ω_1 . Conversely, a detached motor may attach to the track ($0 \rightarrow 1$) with transition rate ω_2 only if located outside this region of size $2a$.

At each instance, the group velocity of the motors is proportional to the total force exerted by the motors (Eq. 2)

$$v(t) = F_{\text{tot}}(t)/\lambda, \quad (3)$$

where the friction coefficient, λ , depends mainly on motors attached to the track and is, therefore, taken proportional to the number of connected motors, $N_c \leq N$ at time t : $\lambda = \lambda_0 N_c$. Because the track is globally a-polar, it is clear that the motors exhibit “back and forth” motion with vanishing mean velocity and displacement. The characteristic time of movement in each direction, τ_{rev} , may nevertheless be macroscopically large. The origin of this feature (which reflects the cooperative character of the motors’ action) can be explained as follows: The stochastic equations of motion of our model system have two identical (except for sign reversal) steady state solutions corresponding to right and left motion of the mechanically coupled motors. Each of

these solutions is characterized by $N_c = N \cdot P$ ($P \leq 1$) connected motors. The connected motors are partitioned to N_+ and $N_- = N_c - N_+ \leq N_+$ motors that, respectively, support and object the motion. Let us define the excess number of motors working in the direction of the motion as $N \cdot \Delta = N_+ - N_-$, where Δ will be termed the “bias parameter”. Notice that P and Δ denote the averages of quantities (which we, respectively, denote by $P(t)$ and $\Delta(t)$) whose values fluctuate in time due to the stochastic binding and unbinding of motors. To switch the direction of motion, $\Delta(t)$ must vanish, and the occurrence probability of this event, $\Pi(\Delta(t) = 0) \sim (\tau_{\text{rev}})^{-1}$. In section 3 we derive an approximate expression for $\Pi(\Delta(t) = 0)$ and show that the mean reversal time of the bidirectional motion increases exponentially with the size of the system:

$$\tau_{\text{rev}} \sim \left[1 - P + \sqrt{P^2 - \Delta^2} \right]^{-N}. \quad (4)$$

Thus, for sufficiently large N , the characteristic reversal time of the bidirectional motion becomes macroscopically large. In the “thermodynamic limit” ($N \rightarrow \infty$), τ_{rev} diverges and the motion persists in the direction chosen at random at the initial time.

The validity of Eq. 4 was recently tested using a motility assay in which myosin II motors drive the motion of globally a-polar actin bundles [9]. In contrast to the predicted exponential dependence of τ_{rev} on the number of working motors, the experimentally measured reversal times showed no dependence on N . The apparent disagreement between the theoretical model and the experimental results can be reconciled by noting that Eq. 4 describes exponential growth of τ_{rev} with N only when P and Δ are themselves independent of N . This is indeed the case in the original model presented by Badoual *et al.* [23], where both the on (ω_2) and off (ω_1) rates do not depend on N . In ref. [9] we introduced a slightly modified version of Badoual’s model, which to a large extent explains the experimentally observed independence of τ_{rev} on N . We argued that the origin of this behavior can be attributed to the tension developed in the actin track due to the action of the attached myosin II motors. An increase in the number of attached motors leads to an increase in the mechanical load which, in turn, leads to an increase in the detachment rate of the motors, as already suggested in models of muscle contraction [29–32]. But unlike most previous studies where the myosin conformational energy was calculated, in ref. [9] we considered the elastic energy stored in the actin track. Within a mean field approximation, this energy scales as $E \sim \langle F_{\text{tot}}^2 \rangle / k_{\text{sp}}$, where k_{sp} is the effective spring constant of the track and F_{tot} is the total force exerted by the motors (see Eq. 3). The total force is the sum of N_c random forces working in opposite directions. Therefore, the mean force $\langle F_{\text{tot}} \rangle = 0$, while $\langle F_{\text{tot}}^2 \rangle$ scales linearly with N_c . The spring constant is inversely proportional to the length of the track, i.e. to the size of the system and to the total number of motors N . We thus conclude that the mean elastic energy of the actin scales like $E/k_B T \sim NN_c$, which means that the detachment of a motor ($N_c \rightarrow N_c - 1$) leads, on average, to an energy gain $dE/k_B T = -\alpha N$ (α is some dimensionless number). This effect can be incorporated within the model by introducing an additional off rate, $\omega_3 = \omega_3^0 \exp(\alpha N)$, outside the gray shaded area in Fig. 1 (i.e., around the potential maxima). Thus, in the modified model, the on and off rates within each unit cell ($-l/2 \leq x \leq +l/2$) of the periodic potential are given by

$$\omega_{\text{on}}(x) = \begin{cases} 0 & |x| \leq a \\ \omega_2 & a < |x| \leq l/2 \end{cases} \quad (5)$$

and

$$\omega_{\text{off}}(x) = \begin{cases} \omega_1 & |x| \leq a \\ \omega_3^0 \exp(\alpha N) & a < |x| \leq l/2. \end{cases} \quad (6)$$

The dependence of $\omega_{\text{off}}(x)$ on N is another, indirect, manifestation of cooperativity between the motors which is mediated through the forces that the motors jointly exert on the actin track. Notice, however, that the cooperative action of the motors does not lead (within the modified model) to correlations between attachment and detachment events of different motors. Moreover, the attachment/detachment rates do not depend on the number of connected motors and, thus, are fixed over time. In ref. [9] we compared the predictions of the original and modified models for model parameters corresponding to the myosin II-actin motility assay. In the former, the reversal times grew exponentially with N from $\tau_{\text{rev}} \sim 1$ sec for $N \sim 1000$, to $\tau_{\text{rev}} \sim 10^3$ sec for $N \sim 3000$. The modified model showed a much better agreement with the experimental results [9]. Specifically, the reversal time did not grow exponentially with N but rather showed a weak maximum around $N \sim 2000$, where $\tau_{\text{rev}} \sim 10$ sec.

In this paper we present a more detailed account of the theoretical model. Several aspects of the model not studied in ref. [9] will be discussed in section 2, including the dynamics on non-random and slightly polar tracks. The steady state solutions of the bidirectional motion are derived analytically in section 3. We use these solutions to estimate the reversal times and compare our analytical predictions with the computational results. We summarize and discuss the results in section 4.

2 Computational results

The model has been presented in details in ref. [9], as well as above in section 1. The model parameters used in this paper are summarized in Table 1. The choice of these values which represent various chemical and physical parameters of the myosin II-actin system is explained in detail in ref. [9]. The model features two new parameters which do not appear in the original model [23]. The off rate ω_3^0 represents the probability of a motor to detach from the track without completing a unit step, and its value was estimated in ref. [9] by noting that in the absence of an elastic load, the probability of such an event is 1-2 orders of magnitude smaller than the complementary probability that the attached motor will execute the step. The constant α depends on the effective elastic spring constant of the basic actin unit (monomer) as well as on the magnitude of the forces that the motors typically apply on the track (see Eq. 5 in ref. [9]). The best fit to the experimental data is achieved with $\alpha = 0.0018$ [9], which gives a weak non-monotonic dependence of τ_{rev} on N . Here we set $\alpha = 0.002$, which gives somewhat poorer agreement with the experimental results but which highlights the differences between Badoual's model [23] and the newly proposed model that takes the elasticity of the actin track into account. As noted above, the consideration of the elastic properties of the actin and the cooperative nature of the action of the working motors considerably improves the results of the original model by replacing the very strong exponential dependence of τ_{rev} on N with a much weaker non-monotonic dependence.

To simulate conditions corresponding to dynamics on a-polar tracks, we randomly chose the direction of random force (the force representing the local polarity of the track, see horizontal

parameter	value
l - period length of the potential	5 nm
q - spacing between adjacent motors	$(5\pi/12)l \sim 6.54$ nm
$2a$ - size of the gray shaded area (see Fig. 7A)	3.8 nm
$2H/l$ - force due to the periodic potential	5 pN
f_{ran} - random force in each unit cell	1 pN
$(\omega_1)^{-1}$ (see Eq. 6)	0.5 msec
$(\omega_2)^{-1}$ (see Eq. 5)	33 msec
$(\omega_3^0)^{-1}$ (see Eq. 6)	7500 msec
α (see Eq. 6)	0.002
λ_0 - friction coefficient per connected motor	85×10^3 kg/sec

Table 1: Values of the model parameters as used in our simulations.

arrows in Fig. 1) in each unit cell, but discarded the tracks at which the sum of random forces did not exactly vanish. We computationally measured characteristic reversal time, τ_{rev} , as a function of N in the range of $400 \leq N \leq 2400$. For each value of N , we generated 40 different realizations of random tracks (each of which consisting of $M \simeq (q/l)N$ units with periodic boundary conditions) and simulated the associated dynamics for a total period of $2 \cdot 10^5$ seconds. During this period of time we followed the changes in the direction of motion and calculated the probability distribution function (PDF) of the reversal times. The characteristic reversal time corresponding to each random track was extracted by fitting the PDF to an exponential form (see Eq. 1), as demonstrated in Fig. 2A. Fig. 2B summarizes our results, where here for each N the reversal time plotted (denoted by $\langle \tau_{\text{rev}} \rangle$) is the average of τ_{rev} calculated for the different track realizations. The error bars represent the standard deviation of τ_{rev} between realizations. The data points depicted in solid circles correspond to $\alpha = 0.002$, while the open circles correspond to $\alpha = 0$, i.e., to the model originally presented in ref. [23] where the on and off rates defined in Eqs. 5 and 6 are independent of N . As predicted by Eq. 4 and indicated by the straight line in Fig. 2B, for $\alpha = 0$ the mean reversal time $\langle \tau_{\text{rev}} \rangle$ exhibits a very strong exponential dependence on N . Because of this very rapid increase of $\langle \tau_{\text{rev}} \rangle$ with N , the reversal times (in the $\alpha = 0$ case) could not be accurately measured for $N > 1800$. Based on the exponential fit (solid line in Fig. 2B), we estimate that for $N = 2400$ the mean reversal time will be of the order of a few hours. In contrast, the calculated $\langle \tau_{\text{rev}} \rangle$ corresponding to $\alpha = 0.002$ show a non-monotonic dependence on N . The computed $\langle \tau_{\text{rev}} \rangle$ are much smaller in this case, and fall below 1 minute for all values of N . In ref. [9], we used slightly different values of the model parameters than those given in Table 1. For the model parameters in ref. [9], the variation of $\langle \tau_{\text{rev}} \rangle$ with N was even weaker than in Fig. 2B and the largest computed $\langle \tau_{\text{rev}} \rangle \leq 12$ sec. These computational results were in a very good quantitative agreement with the experimental results of the in vivo actin-myosin motility assay.

Our simulations reveal surprisingly large variations in the τ_{rev} values between random tracks of similar size (see error bars in Fig. 2B). The origin of these variations lies in the fact that the spacing between motors is larger than the periodicity of the ratchet potential ($q > l$) and, thus, only N out of $M \simeq (q/l)N$ unit cells are ‘‘occupied’’ with motors (which may be either connected

or disconnected) at each instance. Thus, although the track is perfectly a-polar and contains an equal number of cells with random forces pointing in both directions, the subset of occupied cells may have net polarity which constantly changes with time as the motors move collectively along the track. The direction of the net polarity of the occupied cells is also the instantaneous preferred direction of motion. Therefore, the temporal variations in the net polarity must be correlated with the changes in the directionality of the motion. We thus expect tracks on which the net polarity changes more frequently to have smaller τ_{rev} . The effect of net polarity fluctuations does not occur when the motion takes place on periodic a-polar tracks, because in this case the equally spaced motors occupy equal number of cells with left- and right-pointing random forces. Therefore, the reversal times on periodic a-polar tracks are expected to be (i) independent of the periodicity of the track, and (ii) larger than the reversal time on random a-polar tracks. These predictions are fully corroborated by the results from simulations with two very distinct periodic tracks - one with period 2 (i.e., where the local random force changes its sign every unit cell) and one with period M (i.e., when the track is divided into two equal domains of opposite polarities). The results from these two sets of simulations are denoted by triangles in Fig. 2B. The reversal times of both periodic tracks are nearly indistinguishable from each other (the differences between them are smaller than the size of the symbols) and are larger than the reversal times measured for all the random tracks of similar size.

What happens when the simulated track is not perfectly a-polar and the number unit cells in which the random force is pointing in one direction is slightly larger than in the opposite direction? Obviously, the nature of motion is expected to gradually change from bidirectional to unidirectional. In order to investigate this transition between two types of dynamics, we simulated the dynamics of motors on tracks in which the fraction of random forces pointing in one direction, p_l , is slightly larger than 0.5. In the simulations, we fixed the number of motors to $N = 1000$ and varied the difference $D = p_l - (1 - p_l) = 2p_l - 1$ between the fractions of random forces pointing in the favored and disfavored directions. For each track, the simulation data was analyzed in a manner similar to that described above for a-polar tracks, i.e., by fitting the PDF of time intervals of unidirectional motion to an exponential function. There is one notable difference, however, between the analysis of the results for a-polar and for slightly polar tracks. In the latter case, two PDFs, one corresponding for each direction of motion, must be generated with different characteristic reversal times. The motion in the preferred direction is characterized by the larger reversal time, $\tau_{\text{rev-l}}$, which increases with D . Conversely, the smaller reversal time, $\tau_{\text{rev-s}}$, corresponding to the motion in the opposite unpreferred direction decreases with D . These observations are summarized in Figs. 3 and 4. In Fig. 3, the PDFs corresponding to tracks with D values varying from 0 to 0.05 are shown. In the a-polar case $D = 0$, the two PDFs coincide with each others, and the velocity histogram (see inset) is bimodal. As D increases, the two PDFs become increasingly different - the one corresponding to the preferred direction of motion becomes flatter (due to the increase in $\tau_{\text{rev-l}}$), while the other one gets more peaked at the origin (as a result of the decrease in $\tau_{\text{rev-s}}$). The fact that the motors spend larger time intervals moving in one direction is also reflected in the corresponding velocity histograms which become less and less symmetric. The results presented in Fig.3 are obtained from simulations of six different track realizations, one for each different value of D . The mean reversal times, $\langle \tau_{\text{rev-l}} \rangle$ and $\langle \tau_{\text{rev-s}} \rangle$, obtained by averaging the reversal times computed for 8 track realizations for each value of D , are shown in Fig. 4. For $D = 0.05$, $\langle \tau_{\text{rev-l}} \rangle \sim 10 \langle \tau_{\text{rev-s}} \rangle$. For even larger values of D ,

the dynamics are essentially unidirectional, as intervals of motion in the unpreferred direction become very rare and short. We, thus, conclude that bidirectional motion can be observed only on a-polar or slightly polar tracks. This conclusion is directly related to the cooperativity of the motors which causes persistent motion that cannot be easily reversed.

3 Analytical treatment

In the following section we use mean field master equations to analyze the bidirectional motion exhibited by our computational model. The mean field approach corresponds to the limit $N \gg 1$ where one can introduce the probability densities $p_{\text{att}}(x)$ and $p_{\text{det}}(x)$ of finding a motor in the attached or detached state, respectively, at position $-l/2 < x \leq l/2$ within the unit cell of the periodic potential. These probability densities are the steady-state solutions of the following set of coupled master equations which govern the transitions between the two connectivity states:

$$\begin{cases} \partial_t p_{\text{att}}(x, t) + v \partial_x p_{\text{att}}(x, t) = -\omega_{\text{off}}(x) p_{\text{att}}(x, t) + \omega_{\text{on}}(x) p_{\text{det}}(x, t) \\ \partial_t p_{\text{det}}(x, t) + v \partial_x p_{\text{det}}(x, t) = -\omega_{\text{on}}(x) p_{\text{det}}(x, t) + \omega_{\text{off}}(x) p_{\text{att}}(x, t). \end{cases} \quad (7)$$

In Eq. 7, $\omega_{\text{on}}(x)$ and $\omega_{\text{off}}(x)$ denote the space-dependent on and off rates, and v is the group velocity of the motors. Because the spacing between the motors is incommensurate with the periodicity of the potential, the total spatial distribution is uniform in x for $N \gg 1$:

$$p_{\text{att}}(x, t) + p_{\text{det}}(x, t) = \frac{1}{l}. \quad (8)$$

Using Eq. 8, together with Eqs. 5 and 6 to define the on and off rates in Eq. 7, the following steady-state equation ($\partial_t p = 0$) can be derived for $p_{\text{att}}(x)$:

$$lv \frac{dp_{\text{att}}(x)}{dx} = \begin{cases} -l\omega_1 p_{\text{att}}(x) & \text{for } |x| \leq a \\ \omega_2 - l(\omega_2 + \omega_3^0 \exp(\alpha N)) p_{\text{att}}(x) & \text{for } a < |x| \leq l/2. \end{cases} \quad (9)$$

Eq 9 should be solved subject to the boundary condition that $p_{\text{att}}(-l/2) = p_{\text{att}}(l/2)$ and the requirement that $p_{\text{att}}(x)$ is continuous anywhere in the interval $-l/2 \leq x \leq l/2$, including at $x = \pm a$. Several solutions are plotted in Fig. 5 for $2a = 0.76l$ (see Table 1), $\omega_3^0 = 0$, and $(\omega_1, \omega_2) = (v/l, v/l)$ (thin solid line), $(5v/l, 5v/l)$ (dashed line), and $(30v/l, 30v/l)$ (thick solid line). The solutions correspond to the case when the motors move to the right ($v > 0$) and, therefore, it is easy to understand why p_{att} reaches its maximum at $x = -a$ [just before the motors enter, from the left, into the central gray-shaded detachment interval ($-a < x < a$)] and its minimum at $x = a$ [just before leaving the central detachment interval through the right side]. We also notice that when the off rate $\omega_1 \gg v/l$, p_{att} drops very rapidly (exponentially) to near zero in the detachment interval. When the attachment rates $\omega_2 \gg v/l$, p_{att} increases exponentially fast for $x > a$ and rapidly reaches the maximum possible value $p_{\text{att}} = 1/l$. The second steady state solution corresponding to the case when the motors move to the left ($v < 0$) is simply a mirror reflection of the first solution with respect to $x = 0$.

The mean fraction of connected motors, P , can be obtained by integrating the function $p_{\text{att}}(x)$ over the interval $-l/2 \leq x \leq l/2$

$$P = \int_{-l/2}^{l/2} p_{\text{att}}(x) dx. \quad (10)$$

The population of connected motors can be divided into two groups: The connected motors which are located left to the minimum of the periodic potential ($-l/2 < x < 0$) experience forces pushing them to the right, i.e., forces directed in their direction of motion. Conversely, attached motors which are located right to the minimum experience forces directed opposite to their direction of motion. Thus, the bias parameter Δ , previously defined as the excess mean fraction of motors supporting the motion, can be related to p_{att} by

$$\Delta = \int_{-l/2}^0 p_{\text{att}}(x) dx - \int_0^{l/2} p_{\text{att}}(x) dx. \quad (11)$$

In order to derive an expression for the reversal time of the dynamics, we now consider the fluctuations of the instantaneous bias parameter, $\Delta(t)$, around the mean value Δ . The motors may switch their direction of motion when $\Delta(t) = 0$, i.e., when the motion momentarily stops. The occurrence probability of such an event can be related to the mean reversal by:

$$\tau_{\text{rev}} \sim [\Pi(\Delta(t) = 0)]^{-1}. \quad (12)$$

To estimate $\Pi(\Delta(t) = 0)$ we proceed by noting that the probability of finding a motor attached left to the minimum of the potential, i.e. a motor experiencing a force directed in the direction of motion, is $P^+ = (P + \Delta)/2$. The probability that a motor is experiencing a force directed opposite to the direction of motion is $P^- = (P - \Delta)/2$. The probability of having N_+ and $N_- \leq N_+$ motors which, respectively, support and object to the motion can thus be approximated by the trinomial distribution function

$$\pi(N_+, N_-) = \frac{N!}{N_+!N_-!(N - N_+ - N_-)!} \left(\frac{P + \Delta}{2}\right)^{N_+} \left(\frac{P - \Delta}{2}\right)^{N_-} (1 - P)^{(N - N_+ - N_-)}. \quad (13)$$

The instantaneous bias is given by $\Delta(t) = (N_+ - N_-)/N$, and the probability that $\Delta(t) = 0$ can be expressed as sum over the relevant terms in Eq. 13 for which $N_- = N_+$

$$\Pi(\Delta(t) = 0) = \sum_{i=0}^{N/2} \pi(i, i) = \sum_{i=0}^{N/2} \frac{N!}{(i!)^2(N - 2i)!} \left(\frac{P^2 - \Delta^2}{4}\right)^i (1 - P)^{(N - 2i)}. \quad (14)$$

Replacing the sum in Eq. 14 by an integral, using Sterling's approximation for factorials, expanding the logarithm of the integrand in a Taylor series (up to second order) around the maximum which is at $i_{\text{max}} = (N/2)\sqrt{P^2 - \Delta^2}/(1 - P + \sqrt{P^2 - \Delta^2})$ and then exponentiating the expansion, and finally extending the limits of integration to $\pm\infty$ (which has a negligible effect on the result for $N \gg 1$) - leads to:

$$\Pi(\Delta(t) = 0) = \left[1 - P + \sqrt{P^2 - \Delta^2}\right]^N \times \int_{-\infty}^{+\infty} dy \exp\left[-\frac{2}{C(1 - C)N} (y - i_{\text{max}})^2\right], \quad (15)$$

where $C = \sqrt{P^2 - \Delta^2}/(1 - P + \sqrt{P^2 - \Delta^2})$. This yields

$$\tau_{\text{rev}} = \frac{2\tau_0}{\Pi(\Delta(t) = 0)} = 2\tau_0 \sqrt{\frac{2}{\pi C(1 - C)N}} \left[1 - P + \sqrt{P^2 - \Delta^2}\right]^{-N}, \quad (16)$$

where τ_0 is some microscopic time scale. (The factor of 2 in the numerator in Eq. 16 is due to the fact that once the motors stop, they have equal probability to move in both directions.) As noted before (see section 1), Eq. 16 predicts an almost exponential dependence of τ_{rev} on N only for constant values of P and Δ , which was the case in ref. [23]. In the more general case, the dependence of τ_{rev} on N can be derived by calculating the values of P and Δ as a function of N and substituting these values into Eq. 16.

To test the validity and accuracy of the analytical expression for τ_{rev} , we take the following steps: (i) set the model parameters l , a , ω_1 , ω_2 , ω_3^0 , and α to the values used in our computer simulations which are given in Table 1, (ii) calculate the probability density p_{att} corresponding to these values (Eq. 9) and use Eqs. 10 and 11 to calculate P and Δ over the range of N studied in the simulations, (iii) substitute the values of P and Δ into Eq. 16, to obtain τ_{rev} as a function of N , (iv) fit the analytical expression for $\tau_{\text{rev}}(N)$ to the simulation results plotted in Fig. 2B. This procedure involves two fitting parameters: the microscopic time scale τ_0 appearing in Eq. 16, and the group velocity v appearing in the steady-state equation (Eq. 9). A seemingly reasonable choice for the latter would be $v = 20$ nm/sec, which is where the velocity histogram of the bidirectional motion is peaked (see inset of Fig. 3A). However, the motors slow down before each change in their direction of the motion; and because these changes in the directionality are fairly rare events, their occurrence probability is likely to be strongly influenced by the short periods of slow motion preceding them. Thus, it can be expected that the best fit of Eq. 16 to the simulation results is achieved for $v < 20$ nm/sec. Indeed, for $v = 8.2$ nm/sec and $\tau_0 = 680$ msec, we obtain the fitting curve shown in Fig. 6A, which is an excellent agreement with our computational results for the reversal times (plotted in Fig. 2B and replotted here in Fig. 6A) over the whole range of values of N investigated ($400 < N < 2400$). The steady state probability density, $p_{\text{att}}(x)$, on the basis of which τ_{rev} was calculated is shown in Fig. 6B for several different values of N ($N = 1000$ - solid line, $N = 2000$ - dashed line, $N = 2500$ - thick solid line). As can be seen from the figure, the detachment rate ω_1 in our simulations is so large that the central detachment interval of the unit cell ($-a < x < a$) is completely depleted of motors. Increasing N leads to a decrease in the effective attachment rate around the potential maximum, which reduces both the number of motors supporting ($-l/2 < x < -a$) and objecting ($a < x < l/2$) the motion and leads to the non-monotonic dependence of τ on N . The fitting value of $\tau_0 = 680$ msec is very close to $\tau^* = l/v = 5 \text{ nm}/(8 \text{ nm/sec}) = 625$ msec, which is the traveling time of the motors within a unit cell of the potential (once we set $v = 8.2$ nm/sec) and, therefore, is also the characteristic time scale at which the motors change their “states” (detached, connected and supporting the motion, connected and objecting the motion). The remarkable agreement between the analytical and simulation results for τ_{rev} should not, however, be allowed to obscure the fact that Eq. 16 is based on a mean field approximation which, in principle, is not suitable for the calculating the probabilities of rare fluctuation events (such as velocity reversals in cooperative bidirectional movement). The agreement is achieved with effective velocity ($v = 8.2$ nm/sec) which is significantly smaller than the typical velocity measured in the simulations ($v = 20$ nm/sec). Therefore, one should not expect the steady state probability density $p_{\text{att}}(x)$ plotted in Fig. 6B to perfectly match the simulations data.

4 Summary

We use a two-state ratchet model to study the cooperative bidirectional motion of myosin II motors on actin tracks with randomly alternating polarities. Our model is an extension of a model previously proposed by Badoual *et al.* to explain the macroscopically large reversal times measured in motility assays [23]. These time scales of velocity reversals are orders of magnitude longer than the microscopic typical stepping times of individual motors and can be understood as a result of collective effects in many-motor systems. The ratchet model that we use assumes that the motors are coupled mechanically but act independently, i.e., their binding to and unbinding from the cytoskeletal track are statistically uncorrelated. These assumptions lead to a predicted exponential increase of τ_{rev} with N , the number of motors. Motivated by recent experiments which exhibit no such dependence of τ_{rev} on N [9], we introduced a modified version of Badoual’s model which accounts for an additional cooperative effect of the molecular motors and which eliminates the exponential increase of τ_{rev} with N . This additional collective effect arises from the forces that the motors jointly exert on the actin and the associated elastic energy which (within a mean field approximation) scales as $E/K_B T \sim NN_C$ (where $N_C < N$ is the number of attached motors). This scaling relationship implies that the typical energy released when a motor is detaching from the track increases linearly with N and, therefore, the detachment rate in many-motor systems should be larger than the detachment rate of individual motors. We show, both computationally and analytically, that when this effect is taken into account and the detachment rate is properly redefined, the characteristic reversal time does not diverge for large N . Instead, τ_{rev} exhibits a much weaker dependence on N and reaches a maximum at intermediate values of N .

While our model definitely improves the agreement with the experimental results (compared to the original model), further improvement is needed in order to eliminate the non-monotonic dependence of τ_{rev} on N . One step in this direction may be to consider other forms of the off-rate ω_3 which are based on more accurate evaluations of the actin elastic energy. In the present work, our analysis is based on a mean field approximation which makes the calculation tractable by assuming that the detachment rate depends only on N (the total number of motors), but not on the instantaneous number of attached motors and their locations along the cytoskeletal track. A full statistical mechanical treatment is feasible only for small systems, which we plan to report in a future publication. As a final remark here we note that the mean field approximation probably leads to over-estimation of the effect of the “track-mediated” elastic interactions on the reversal times (which may explain the decrease in τ_{rev} for large N). In a non-mean-field calculation the motors which release higher energy will detach at higher rates, and the detachment of these “energetic” motors will lead to the release of much of the elastic energy stored in the actin track. By contrast, in the mean field approximation the contribution of all the connected motors to the energy is the same. Therefore, within the mean-field approximation, a larger number of motors must be disconnected at a higher frequency, which increases the “stochastic noise” in the system that reduced τ_{rev} .

We thank Haim Diamant and Yariv Kafri for useful discussions. A.B.G wishes to thank the Joseph and May Winston Foundation Career Development Chair in Chemical Engineering, the Israel Cancer Association (grant No. 20070020B) and the Israel Science Foundation (grant No. 551/04).

References

- [1] R. Vale, *Cell* **112**, 467 (2003).
- [2] M. A. Geeves and K. C. Holmes, *Annu. Rev. Biochem.* **68**, 687 (1999).
- [3] B. Feierbach and F. Chang, *Curr. Opin. Microbiol.* **4**, 713 (2001).
- [4] K. E. Machine and J. W. S. Pringle, *Proc. R Soc. Lond. B Biol. Sci.* **151**, 204 (1959).
- [5] S. Camalet and F. Jülicher *New J. Phys.*, **2**, 1 (2000).
- [6] C. J. Brokaw, *Proc. Natl. Acad. Sci. USA* **72**, 3102 (1975).
- [7] G. Koster, M. VanDuijn, B. Hofs and M. Dogterom, *Proc. Natl. Acad. Sci. USA* **100**, 15583 (2003).
- [8] C. Leduc, O. Campás, K. B. Zeldovic, A. Roux, P. Jolimaitre, L. Bourel-Bonnet, B. Goud, J.-F. Joanny, P. Bassereau and J. Prost, *Proc. Natl. Acad. Sci. USA* **101**, 17096 (2004).
- [9] B. Gilboa, D. Gillo, O. Farago and A. Bernheim-Groswasser, *Soft Matter* **5**, 2223 (2009).
- [10] S. A. Endow and H. Higuchi, *Nature* **406**, 913 (2000).
- [11] L. Tao, A. Mogliner, G. Civelekoglu-Scholey, R. Wollman, J. Evans, H. Stahlberg and J. M. Scholey, *Curr. Bio.* **16**, 2293 (2006).
- [12] D. Riveline, A. Ott, F. Jülicher, D. A. Winklemann, O. Cardoso, J. J. Lacap??e, S. Magnúsdóttir, J. L. Viovy, L. Gorre-Talini and J. Prost, *Eur. Biophys. J.* **27**, 403 (1998).
- [13] S. P. Gross, M. Carolina Tuma, S. W. Deacon, A. S. Serpinskaya, A. R. Reilein and V. L. Gelfand, *J. Cell Biol.* **156**, 855 (2002).
- [14] D. Chowdhury, *Phys. Scripta* **T106**, 13 (2003).
- [15] A. Parmeggiani, T. Franosch and E. Frey, *Phys. Rev. Lett.* **90**, 086601 (2003).
- [16] O. Campás, Y. Kafri, K. B. Zeldovich, J. Casademunt and J.-F. Joanny, *Phys. Rev. Lett.* **97**, 038101 (2006).
- [17] S. Muhuri and I. Pagonabarraga, *Europhys. Lett.* **84**, 58009 (2008).
- [18] D. Chowdhury, A. Garai and J. S. Wang, *Phys. Rev. E* **77**, 050902(R) (2008).
- [19] D. G. Lichtenthaler and C. Goldman, preprint cond-mat:0803.2732 (2008).
- [20] M. Ebbinghaus, L. Santen, preprint cond-mat:0901.0183 (2009).
- [21] F. Jülicher and J. Prost, *Phys. Rev. Lett.* **75**, 2618 (1995).
- [22] F. Jülicher and J. Prost, *Phys. Rev. Lett.* **78**, 4510 (1997).

- [23] M. Badoual, F. Jülicher and J. Prost, *Proc. Natl. Acad. Sci. USA* **99**, 6696 (2002).
- [24] R. M. da Silva, C. C. de Souza Silva and S. Coutinho, *Phys. Rev. E* **78**, 061131 (2008).
- [25] S. Klumpp and R. Lipowsky, *Proc. Natl. Acad. Sci. USA* **102**, 17284 (2005).
- [26] M. J. I. Müller, S. Klumpp and R. Lipowsky, *Proc. Natl. Acad. Sci. USA* **105**, 4609 (2008).
- [27] Y. Zhang, preprint cond-mat:0901.0350 (2009).
- [28] D. Hexner and Y. Kafri, preprint cond-mat:0903.0312 (2009).
- [29] D. A. Smith and M. A. Geeves, *Biophys. J.* **69**, 524- (1995).
- [30] T. A. J Duke, *Proc. Natl. Acad. Sci. USA* **96**, 2770 (1999).
- [31] G. Lan and S. X. Sun, *Biophys. J.* **88**, 4107 (2005).
- [32] R. E. L De Ville and E. Venden-Eijnden, *Bull. Math. Bio.* **70**, 484 (2008).

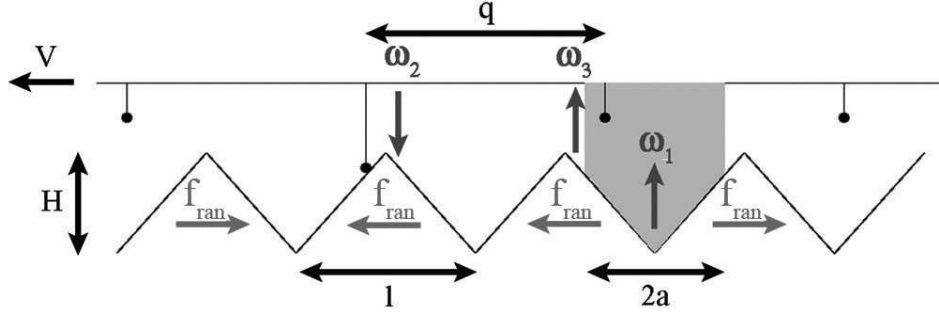


Figure 1: N point particles (representing the motors) are connected to a rigid rod with equal spacing q . The motors interact with the actin track via a periodic, symmetric, saw-tooth potential with period l and height H . In each periodic unit, there is a random force of size f_{ran} , pointing either to the right or to the left. The motors are subject to these forces only if connected to the track. The detachment rate ω_1 is localized in the shaded area of length $2a < l$, while the attachment rate ω_2 is located outside of this region. The off rate ω_3 is permitted only outside the gray shaded area.

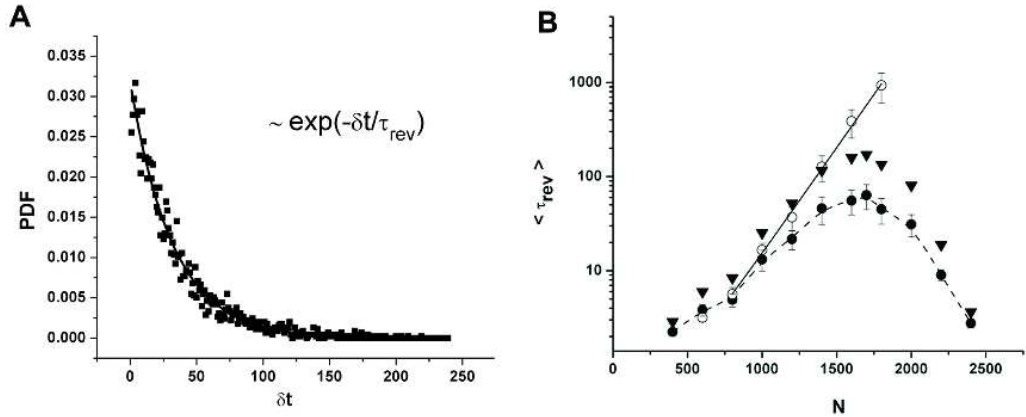


Figure 2: (A) The probability distribution function (PDF) of reversal times corresponding to one track realization. The distribution is fitted by a single exponential decay function - see Eq. 1. (B) The mean reversal time $\langle \tau_{\text{rev}} \rangle$ as a function of the number of motors N . For each value of N , the calculation of $\langle \tau_{\text{rev}} \rangle$ is based on simulations of 40 different track realizations, where the error bars represent the standard deviation of τ_{rev} between realizations. The solid and open circles denote the results corresponding to $\alpha = 0.002$ (our model) and $\alpha = 0$ (original model presented in ref. [23]), respectively. In the latter case $\langle \tau_{\text{rev}} \rangle$ increases exponentially with N (as indicated by the solid straight line), while in the former case $\langle \tau_{\text{rev}} \rangle$ exhibits a non-monotonic behavior (as indicated by the dashed line which serves as a guide to the eye) and reaches considerably lower values. The triangles denote the results for periodic tracks whose reversal times are always larger than those measured on random tracks.

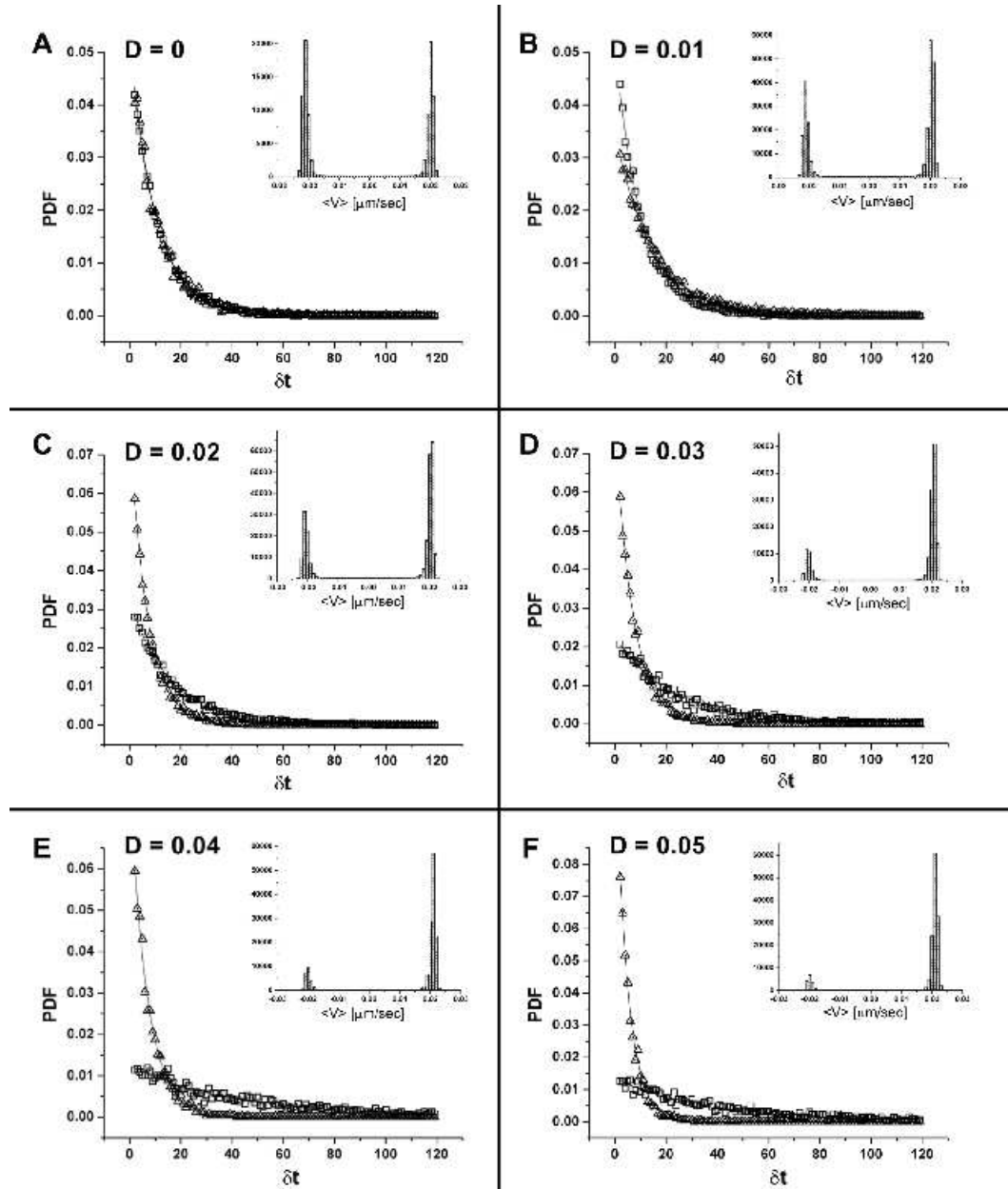


Figure 3: The probability distribution functions (PDF) of reversal times corresponding to $N = 1000$ motors moving on slightly polar tracks. The variable D denotes the difference between the fraction of random forces pointing in the favored and disfavored directions. The motion in the favored and disfavored directions are analyzed by different PDFs, each of which can be fitted by a single exponential form but with distinct reversal times (except for $D = 0$ where the two PDFs coincide with each other). The insets show the velocity histogram corresponding to each value of D . As D increases, the histograms become less and less symmetric.

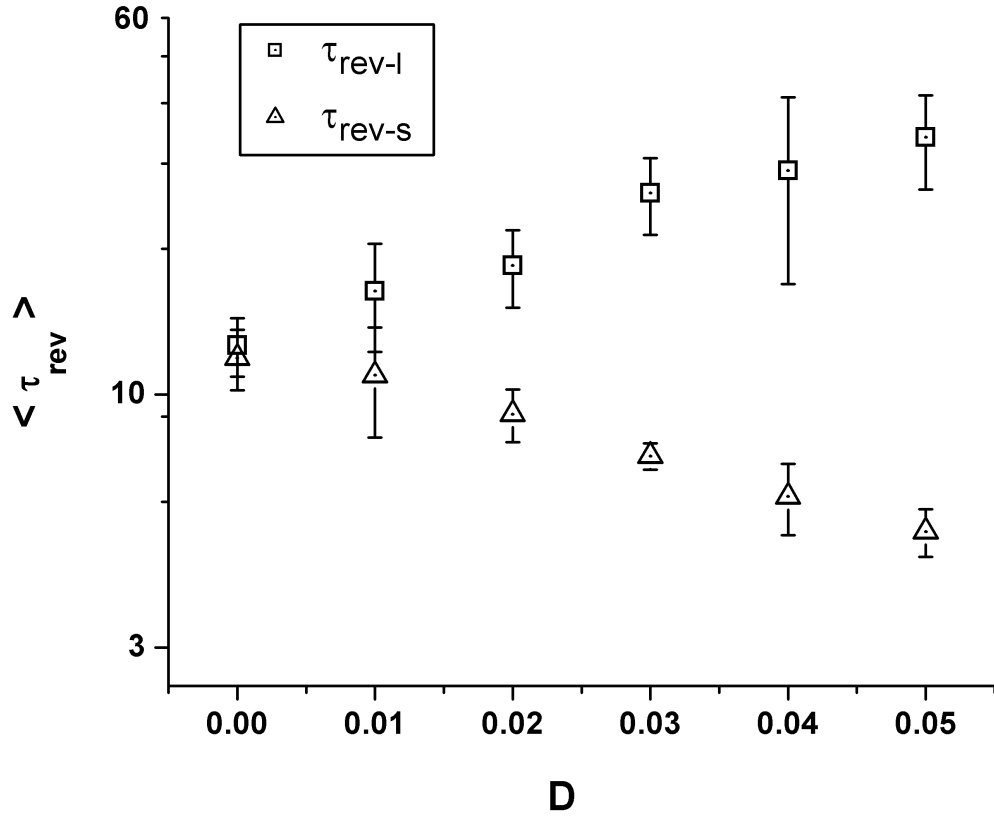


Figure 4: The mean reversal times (computed based on simulations of 8 track realizations with $N = 1000$ motors) as a function of D , the difference between the fraction of random forces along the track which point in the favored and disfavored directions. The motion in the favored and disfavored directions are characterized by the larger ($\tau_{\text{rev-l}}$) and smaller ($\tau_{\text{rev-s}}$) reversal times, respectively.

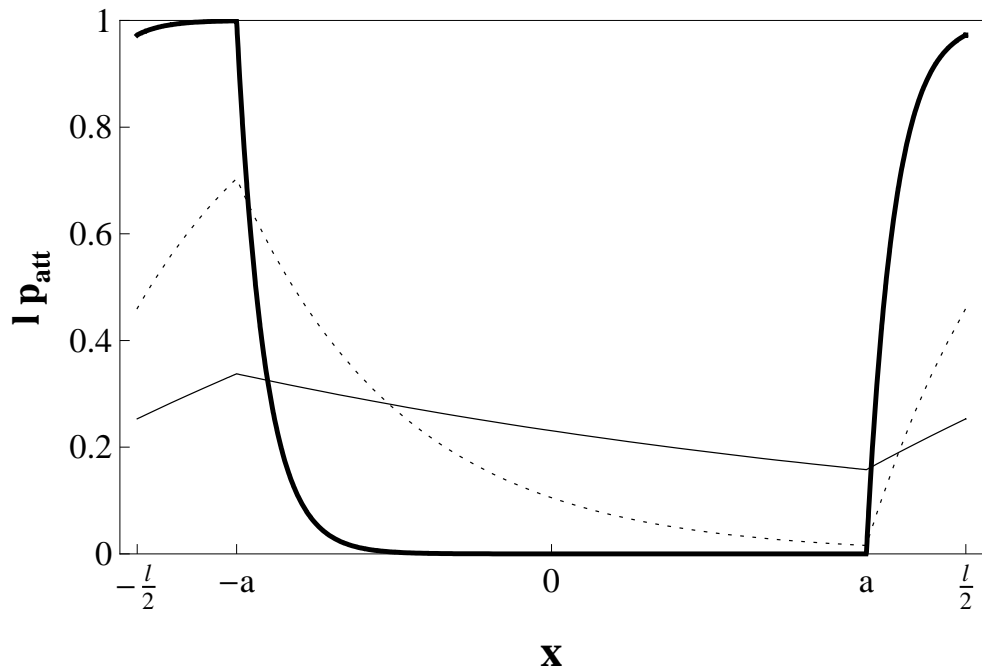


Figure 5: The steady state probability density, p_{att} , as a function of x , the position within a unit cell of the periodic potential. The functions plotted in the figure correspond to $2a = 0.76l$, $\omega_3^0 = 0$, and $(\omega_1, \omega_2) = (v/l, v/l)$ - thin solid line, $(\omega_1, \omega_2) = (5v/l, 5v/l)$ - dashed line, $(\omega_1, \omega_2) = (30v/l, 30v/l)$ - thick solid line.

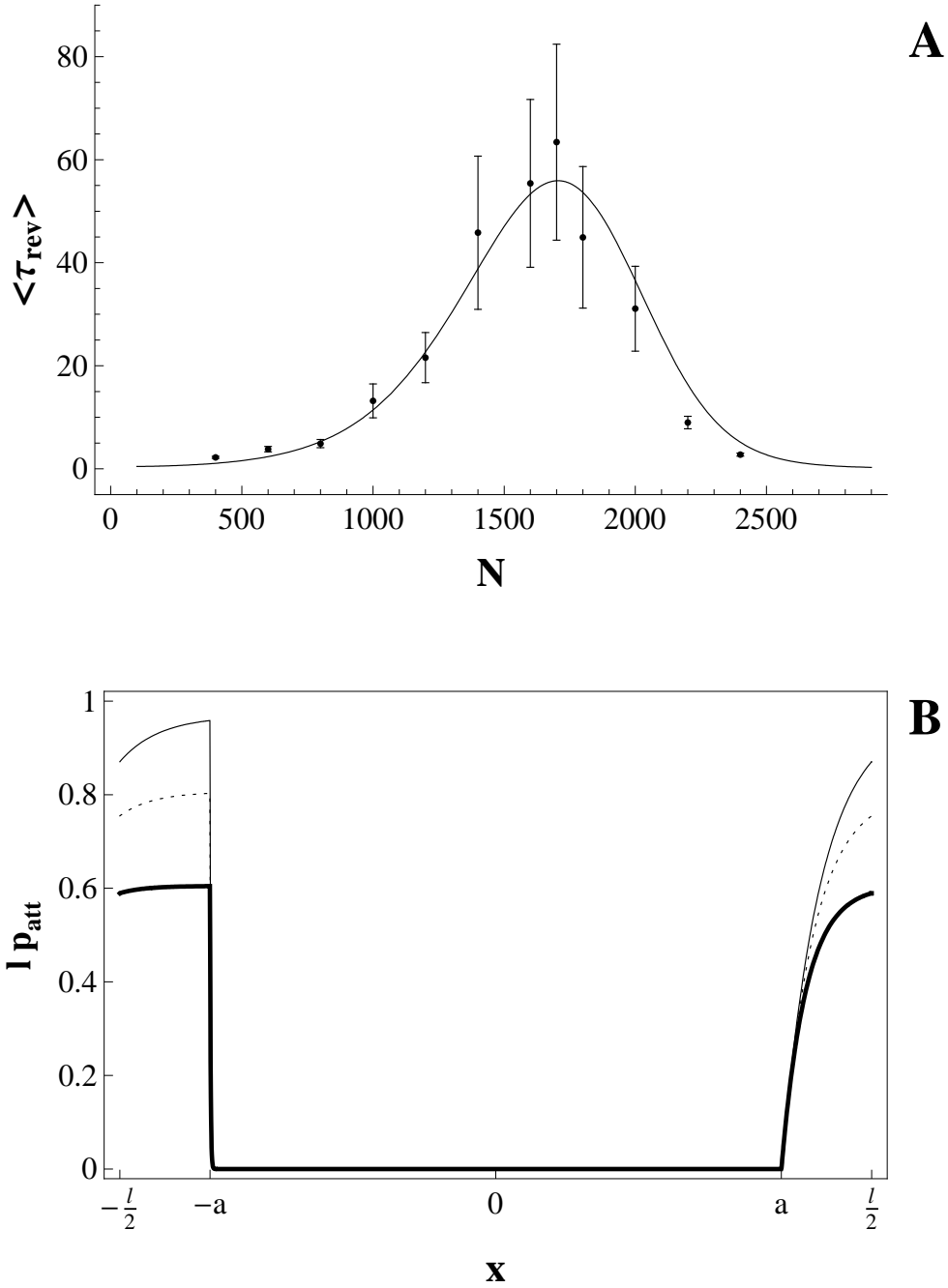


Figure 6: (A) The reversal time $\langle \tau_{\text{rev}} \rangle$ function of the number of motors N . The circles denote the simulations results (replotted from Fig. 2). The curve is a fit of the results to Eq. 16, with $\tau_0 = 680$ msec and $v = 8.2$ nm/sec. (B) The steady state probability density $p_{\text{att}}(x)$ computed for several values of N ($N = 1000$ - solid line, $N = 2000$ - dashed line, $N = 2500$ - thick solid line). The group velocity of the motors is $v = 8.2$ nm/sec [as in (A), above], while the model parameters are set to the values used in our simulations (see Table 1).